Effect of emitter thickness on the spectral shape of heterojunction interfacial workfunction internal photoemission detectors

S. G. Matsik,[1] R. C. Jayasinghe,[1] A. B. Weerasekara,[1] A. G. U. Perera,[1,a)]
E. H. Linfield,[2] S. P. Khanna,[2] M. Lachab,[2] and H. C. Liu[3]
[1]*Department of Physics and Astronomy, Georgia State University, Atlanta, Georgia 30303, USA*
[2]*School of Electronic and Electrical Engineering, University of Leeds, Leeds LS2 9JT, United Kingdom*
[3]*Institute for Microstructural Sciences, National Research Council, Ottawa K1A 0R6, Canada*

(Received 23 March 2009; accepted 14 May 2009; published online 14 July 2009)

Results are presented showing the effect of emitter layer thickness on the shape of the spectral response of heterojunction interfacial workfunction internal photoemission detectors. The results confirm that thicker emitters increase the response at shorter wavelengths. A model is developed to explain the experimentally observed blueshift in the peak wavelength with increased emitter thickness, using a combination of hot-cold carrier scattering and phonon emission processes. The study provides a tool for designing detectors exhibiting different peak responses, as demonstrated by evaluating the design parameters for the 8–14 μm spectral range. © *2009 American Institute of Physics*. [DOI: 10.1063/1.3153954]

Tailoring the response of solid state infrared (IR) detectors for specific applications has become increasingly important recently. The heterojunction interfacial-workfunction internal photoemission (HEIWIP) detector[1,2] is a specific type of device that has been developed, which consists of several highly doped emitter and undoped barrier layers placed between highly doped contacts. Recent results from *n*-type HEIWIP structures show sensitivities at wavelengths up to 93 μm.[3,4]

The basic model[5] for the response of HEIWIP detectors consists of three mechanisms; absorption, internal photoemission, and collection of the photocarriers. While significant progress has been achieved[6] in optimizing the modeling of the absorption, there are few studies on the other two factors. Typically the emission is calculated using an escape cone model,[7] while the collection efficiency is either taken as 1 or is determined empirically after the detectors have been tested. Here, a detailed study of the photoemission efficiency is carried out allowing the optimization of detectors for specific applications.

Two heterostructures (Table I) were designed to study the effects of emitter thickness variation on the detector performance. Each structure consisted of 1×10^{18} cm^{-3} *n*-doped GaAs emitters and undoped $Al_{0.12}Ga_{0.88}As$ barriers, placed between 5×10^{18} cm^{-3} *n*-doped contacts. One structure (L200) had 12 periods of 20 nm emitters and 80 nm barriers; the other structure (L202) had 4 periods of 60 nm emitters and 240 nm barriers. The total emitter thickness and the total overall thickness of the structures were kept constant. All other parameters were kept the same.

The model assumes that the light intensity does not vary through the thickness of an emitter, the variation being only a few percent for an emitter thickness of 60 nm. Hence, the photoexcited carriers are generated uniformly throughout the emitter, allowing the absorption and carrier escape probabilities to be calculated separately and then multiplied to obtain a total probability. Four classes of scattering processes are considered to determine the photoemission efficiency. These include the processes in which the photoexcited carrier energy is (i) not changed, such as ionized impurity scattering; (ii) reduced owing to emission of a phonon; (iii) increased owing to the absorption of a phonon; and (iv) reduced by photoexcited carriers losing energy and cold carriers gaining energy during a collision. At low temperatures ($\sim$5 K) used for the spectral response measurements, the phonon absorption processes can be ignored. The scattering length for phonon emission found from calculations[9] is greater than the individual emitter thickness indicating a minor impact on the shape of the spectral responsivity. Scattering without any change in the carrier energy switches carriers between the inside and outside the escape cone, defined by $E_z=E\cos\theta$, i.e., the transverse energy, is greater or less than the barrier height, respectively. In the absence of any edge effects, this process is balanced, with as many carriers scattering into the cone as out of the cone. However, near the barrier, where carriers can escape into the next period of the structure, this carrier-carrier scattering mechanism can lead to a net increase in the number of escaping carriers. Hence ionized impurity scattering, phonon emission scattering, and scattering of the hot and cold carriers are included in the model.

The absorption coefficient for the *j*th layer in the structure was obtained from the complex dielectric constant in the form

$$\varepsilon_j(\omega)=\varepsilon_{\infty,j}\left[1-\frac{\omega_{p,j}^2}{\omega(\omega+i\omega_{0,j})}\right]+\frac{\omega_{\mathrm{TO},j}^2(\varepsilon_{s,j}-\varepsilon_{\infty,j})}{\omega_{\mathrm{TO},j}^2-\omega^2-i\omega\gamma_j}. \quad (1)$$

Here ε_s and ε_∞ are the static and high frequency dielectric constants of the intrinsic semiconductor, $\omega_0=1/\tau$ is the free carrier damping constant, where τ is a relaxation time, ω_{TO} is the transverse optical phonon frequency, and γ is a phonon damping coefficient. The plasma frequency of free carriers with effective mass m^* and concentration N_p is given by

a)Electronic mail: uperera@gsu.edu.

 © 2009 American Institute of Physics

Author complimentary copy. Redistribution subject to AIP license or copyright, see http://jap.aip.org/jap/copyright.jsp

TABLE I. The design parameters of the structures used for studying the effects of emitter thickness. All structures had contacts n doped to 5×10^{18} cm^{-3}, emitters n doped to 1×10^{18} cm^{-3}, and an Al fraction in the barrier of $x=0.12$. Also given are the calculated peak response wavelength, λ_p, of the free carrier response and the maximum responsivity, R_p, obtained for the model.

Sample	Periods	Emitter thickness (nm)	Barrier thickness (nm)	Total thicknes (μm)	Calculated λ_p (μm)	Calculated R_p (mA/W)
L200	12	20	80	1.2	18	1.0
L202	4	60	240	1.2	12	1.3

$\omega_p=\sqrt{N_p q^2/\varepsilon_o\varepsilon_\infty m^*}$, where q is the magnitude of the electron charge. The photon absorption is then calculated as

$$\eta_a = 2\frac{\omega}{c}\,\mathrm{Im}(\varepsilon(\omega))\frac{1}{|E_0|^2}\int_0^W |E(z)|^2 dz$$
$$= 2\frac{\omega}{c}\,\mathrm{Im}(\varepsilon(\omega))\frac{\overline{|E|^2}}{|E_0|^2}W, \qquad (2)$$

where $\mathrm{Im}(\varepsilon(\omega))$ is the imaginary part of the dielectric function, ω is the wave frequency, E is the electric field of the electromagnetic wave inside the layer, E_0 is the electric field of the incident radiation, and W is the thickness of the emitter layer.

Photoemission efficiency calculation is divided into transport of electrons to the interface and the actual emission at the interface which is well understood.[7] The calculated escape probability is multiplied by the absorption in the emitter to obtain the spectral response. The escape probability of an electron for a given incident photon energy was determined by exciting a carrier at random (in terms of its initial position, energy, and direction) from the Fermi distribution in the emitter. The excited carrier propagates through the emitter with a scattering probability for each process given by

$$p_i = dx/l_i, \qquad (3)$$

where dx is the distance traveled in a single step, and l_i is the scattering length for the ith process. For each step, the step length was randomly selected. At the end of each step, it was checked whether the carrier had reached the barrier and escaped. Any carrier reaching the barrier without sufficient energy (associated with motion perpendicular to the barrier) to escape was assumed to be reflected back into the emitter. If the carrier did not escape, the scattering process was selected based on the scattering probabilities. For processes (i) and (ii), calculated[9] scattering time was used to determine the scattering probability. For process (iv), associated with hot-cold carrier scattering, the scattering length was taken as a fitting parameter. It was assumed that both carriers would have random directions after scattering, without changing the center of mass velocity. The total energy of the carriers was conserved, and the initial cold carrier energy was selected randomly from the cold carrier energy distribution. The carrier propagation and scattering process were repeated until the total carrier energy fell to less than the barrier height. The escape probability was determined by averaging over a large number of trials. While not giving exact fits to the experimental results, these assumptions were sufficient to demonstrate the main qualitative features of the observed response and allow determination of the scattering length for the hot-cold carrier collisions. A more detailed model of the scattering events, including many body effects, is needed for a quantitative fit to the data.

The effect of the hot-cold carrier scattering[8] will depend on the energy of the hot carriers. Hot carriers with energies that are just sufficient to pass over the barrier will be trapped after losing energy. Hence, for the long-wavelength portion of the spectrum, it is expected that once the photoexcited carriers have to travel more than one scattering length, they will not be able to escape on reaching the interface and hence will not contribute to the response. This means that the spectral response shape near the long-wavelength threshold is the same for both structures. In contrast, for shorter wavelength excitation, the electrons would be expected to escape after multiple collisions.

The structures were grown by molecular beam epitaxy and detectors were fabricated using wet chemical etching to produce square mesa's of side 400 μm. Ni/Ge/Au was deposited on the top and bottom contact layers, and annealed to form Ohmic contacts. The spectra of the detectors were measured at low temperature using a Fourier transform IR spectrometer and a broadband source, with the responsivity calibrated using a silicon composite bolometer. The response for a bias of ~300 mV for both structures is shown in Fig. 1. The most significant feature in these curves is the large increase in response for sample L202, which has thicker emitter layers, at wavelengths significantly lower than the threshold wavelength with a dropping response at longer wavelengths. The peak response detected in the spectra at ~20 μm (particularly noticeable in L200) is believed to be the result of light absorption by impurities. In addition, there is a reduced response at ~18 μm for both samples as a result of an AlAs-like phonon associated with the barriers.

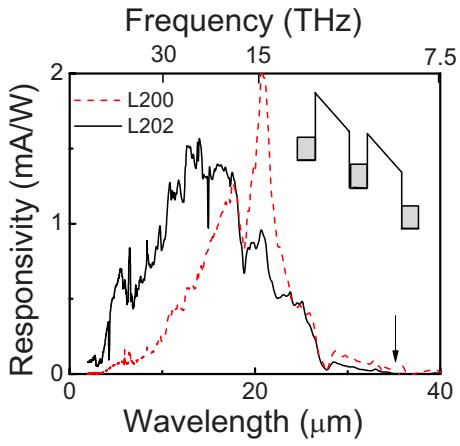

FIG. 1. (Color online) The experimentally measured spectra at a 300 mV bias and 4.2 K for the two samples. The response of L200 was greater at longer wavelengths, probably as a result of the increased gain leading to a shift in the peak response from 20.8 to ~13 μm as well as an increase in the FWHM. Inset: A schematic band diagram for the detector.

Author complimentary copy. Redistribution subject to AIP license or copyright, see http://jap.aip.org/jap/copyright.jsp

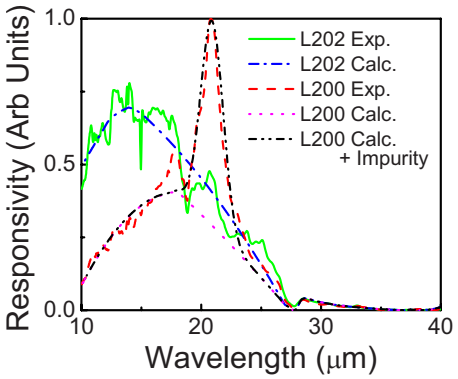

FIG. 2. (Color online) The experimentally measured spectra at 4.2 K, and the calculated spectra with the scattering effects included, for the samples with the 20 nm (L200) and the 60 nm (L202) emitter thicknesses. The scattering length for the hot-cold carrier process was adjusted to fit the sample with thicker emitters, and the same value was then used to model the sample with thinner emitters. Good agreement is obtained for sample L202, while there is deviation in the results for L200 owing to the impurity peak. The model shows an increased response observed at short wavelengths for the thicker emitter sample. The sharp drop observed near 18 μm is due to the presence of an AlAs-like phonon.

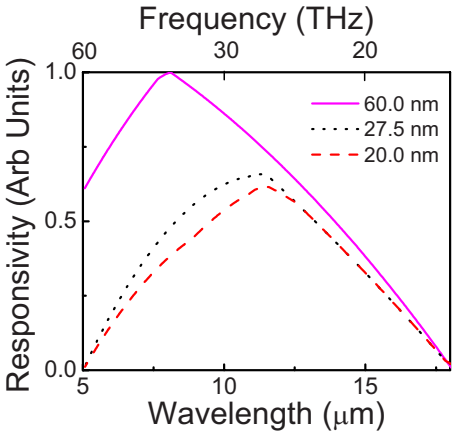

FIG. 3. (Color online) The spectral response for detectors optimized for the 8–14 μm region, showing the effect of emitter thicknesses.

The response at the longer wavelengths should be nearly the same for both samples, as the effects of scattering in the thicker emitters should not contribute in this case. Thus the differences must be attributed to the differences in the gain factor associated with the different numbers of emitters and the different barrier thicknesses. As the response at wavelengths longer than ~35 μm from sample L202 with only 4 emitters was less than that for sample L200 with 12 emitters, it appears that the gain for sample L200 is larger even though the emitters are thinner.

A comparison between the model and experimental data for both samples is shown in Fig. 2. The calculated response was obtained using a phonon emission scattering length of ~80 nm and a hot-cold carrier scattering length of ~15 nm. These fitting parameters were obtained for sample L202 and then applied to sample L200. While these values fit the response for sample L202 well, the fit of sample L200, with its thinner emitters, is much poorer (see Fig. 2). The fit is improved significantly by the inclusion of the impurity peak on the long-wavelength side of the spectrum. The quality of the fit can also be increased by improving the scattering model assumed for the hot-cold carrier interactions. In particular, the model assumes that this interaction consists of isolated scattering events involving only two carriers at a time. However, the hot carrier minimum separation for which large angle scattering occurs is ~15–20 nm, while the separation of the cold carriers is only ~10 nm. This implies that the hot carriers will be interacting with more than one cold carrier at the same time, affecting the scattering angles and the energy transferred between carriers. Inclusion of many body effects in the scattering, together with the impurity interaction, should lead to a better fit to the observed spectral response. However, even without these corrections, the model shows a significant enhancement of the response for the detector with thicker emitters (L202, Fig. 2) at shorter wavelengths. The peak response wavelength and peak responsivity predicted by the model are summarized in Table I. Increasing the emitter thickness from 20 to 60 nm has shifted the peak response wavelength from 18 to 12 μm while also increasing the peak response by 30%.

Increasing the emitter thickness is expected to increase the response at all wavelengths. For carriers with energies only slightly above the barrier height, however, there is a minimal contribution to carrier escape through scattering. The enhancement of response with increased thickness will, therefore, become negligible, once the average photoexcited carrier transport distance in the emitter exceeds the scattering length. For carriers with higher energies, where gain through scattering is possible, the carrier response will increase rapidly once gain occurs, tending to a constant value at larger thicknesses when scattered carriers can no longer escape. The predicted variation of spectral response for a detector operating in the 5–15 μm range is shown in Fig. 3. (For the data in this figure, the Al fraction of the barriers has been reduced to 11% giving λ_t of 18.5 μm.) For the 20 nm thick emitters used previously, the full width at half maximum (FWHM) of the detector would only cover the 8–14 μm range. Increasing the thickness of the 1×10^{18} cm^{-3} doped emitters from 20 to 27.5 nm extends the short wavelength range down to 7 μm. Further increase in the emitter thickness to 60 nm will cover an optical range of <5 μm up to 15 μm. Indeed this concept can be extended to design detectors for various ranges including the two atmospheric windows and the terahertz region. For example, a detector with a 100 μm zero response threshold would have the FWHM points at 45–75 μm for a 20 nm thick emitter. By increasing the emitter thickness to 60 nm, the FWHM would be extended to cover the range 25–75 μm. Similarly, for a 300 μm threshold detector, increasing the emitter thickness from 20 to 60 nm would change the FWHM range from 140–220 μm to 60–220 μm. This capability would allow the detector response width to be tailored for specific applications.

In summary, the FWHM increases and the peak wavelength shifts to shorter wavelengths as the emitter thickness increases (Table II) allowing the design of detectors for different peak wavelength with variable FWHM. These results allow the design of detectors with specific peak wavelength and FWHM responsivities. For example, a 14 μm threshold

Author complimentary copy. Redistribution subject to AIP license or copyright, see http://jap.aip.org/jap/copyright.jsp

TABLE II. The calculated detector peak wavelength, λ_p, and FWHM for different emitter thicknesses and for threshold wavelengths, λ_t, of 37 and 18.5 μm.

Emitter thickness (nm)	λ_t (μm)	λ_p (μm)	FWHM (μm)
20	37	17.5	10
40	37	16	12
60	37	14	15
80	37	12	20
20	18.5	12	7
27.5	18.5	12	7.5
60	18.5	8	9

detector with 27.5 nm thick emitters and $Al_{0.11}Ga_{0.89}As$ barriers would cover the 7–14 μm range with a peak response at 12 μm. This detector would have the majority of its response at the short end of the wavelength range. The results imply that when designing detectors for specific applications, both the emitter thickness and the threshold wavelength should be considered. If a narrow response is desired, thin emitters with a shorter threshold wavelength should be chosen. For a broader response, thicker emitters with a longer threshold wavelength are preferred.

This work was supported in part by the US NSF under Grant No. ECS-0553051, the Georgia Research Alliance, and by the EPSRC (UK).

[1]A. G. U. Perera, S. G. Matsik, B. Yaldiz, H. C. Liu, A. Shen, M. Gao, Z. R. Wasilewski, and M. Buchanan, Appl. Phys. Lett. **78**, 2241 (2001).
[2]M. B. M. Rinzan, A. G. U. Perera, S. G. Matsik, H. C. Liu, Z. R. Wasilewski, and M. Buchanan, Appl. Phys. Lett. **86**, 071112 (2005).
[3]A. Weerasekara, M. Rinzan, S. Matsik, A. G. U. Perera, M. Buchanan, H. C. Liu, G. von Winckel, A. Stintz, and S. Krishna, Opt. Lett. **32**, 1335 (2007).
[4]S. Jit, A. B. Weerasekara, R. C. Jayasinghe, S. G. Matsik, A. G. U. Perera, M. Buchanan, G. I. Sproule, H. C. Liu, A. Stintz, S. Krishna, S. P. Khanna, M. Lachab, and E. H. Linfield, IEEE Electron Device Lett. **29**, 1090 (2008).
[5]D. G. Esaev, M. B. M. Rinzan, S. G. Matsik, and A. G. U. Perera, J. Appl. Phys. **96**, 4588 (2004).
[6]D. G. Esaev, S. G. Matsik, M. B. M. Rinzan, A. G. U. Perera, H. C. Liu, and M. Buchanan, J. Appl. Phys. **93**, 1879 (2003).
[7]R. Williams, in *Semiconductors and Semimetals*, edited by R. K. Willardson and A. C. Beer (Academic, New York, 1970), Vol. 6, p. 97.
[8]J. M. Mooney and J. Silverman, IEEE Trans. Electron Devices **32**, 33 (1985).
[9]T. Brudevoll, T. A. Fjeldly, J. Baek, and M. S. Shur, J. Appl. Phys. **67**, 7373 (1990).

Author complimentary copy. Redistribution subject to AIP license or copyright, see http://jap.aip.org/jap/copyright.jsp